*mathematics*

MDPI

*Article*

# A Novel Axial Load Inversion Method for Rock Bolts Based on the Surface Strain of a Bearing Plate

**Yongchao Lei [1,2,3], Xingliang Xu [1,3,4,*], Suchuan Tian [1] and Hao Shi [4]**

[1] State Key Laboratory for Fine Exploration and Intelligent Development of Coal Resources, China University of Mining and Technology, Xuzhou 221116, China; leiyongchao@cumt.edu.cn (Y.L.); tiansc@cumt.edu.cn (S.T.)
[2] Henan Energy Group Co., Ltd., Zhengzhou 450046, China
[3] Mining Department, Xinjiang Institute of Engineering, Urumqi 830023, China
[4] School of Mines, China University of Mining and Technology, Xuzhou 221116, China; shihaoxs@cumt.edu.cn
* Correspondence: xlxucumt@cumt.edu.cn

**Abstract:** Anchor rock bolts are among the essential support components employed in coal mine support engineering. Measuring the axial load of the supporting anchor bolts constitutes an important foundation for evaluating the support effect and the mechanical state of the surrounding rock. The existing methods for measuring the axial load of rock bolts have difficulty meeting the actual demands in terms of accuracy and means. Therefore, we propose a novel inverse method for determining the axial load of rock bolts. On the basis of the dynamic relationship between the axial load of the anchor bolt and the strain of the plate, a calculation model for the inverse analysis of the axial load from the plate strain is presented, and it is verified and corrected through finite element analysis and indoor physical experiments. By combining the calculation model with the digital image correlation method, a low costinversion of the axial load of the anchor bolt in actual support engineering is achieved. The experimental results demonstrate that the average errors of the load inversion of anchor bolts in three different states via the theory and method proposed in this paper are less than 8.8% (4 kN), 3.6% (3.2 kN), and 14.7% (5.5 kN), respectively, and the average error of the axial load of the rock bolts in the proposed method is only 4.23 kN. It possesses relatively high accuracy and can be effectively applied in the actual production processes of mines.

**Keywords:** rock bolts; axial load inversion; digital image correlation; bolt plate; support engineering

**MSC:** 68U05

check for updates

**Citation:** Lei, Y.; Xu, X.; Tian, S.; Shi, H. A Novel Axial Load Inversion Method for Rock Bolts Based on the Surface Strain of a Bearing Plate. *Mathematics* **2024**, *12*, 3480. https://doi.org/10.3390/math12223480

Academic Editor: David Greiner

Received: 28 September 2024
Revised: 5 November 2024
Accepted: 6 November 2024
Published: 7 November 2024

**Copyright:** © 2024 by the authors. Licensee MDPI, Basel, Switzerland. This article is an open access article distributed under the terms and conditions of the Creative Commons Attribution (CC BY) license (https://creativecommons.org/licenses/by/4.0/).

## 1. Introduction

Rock bolt support is a commonly used support method in tunnel excavation, resource excavation, underground space construction, and other fields. In particular, bolt support plays a highly significant role in roadway driving and coal mining [1–3]. However, the essence of supporting the surrounding rock is controlling the mechanical state of the surrounding rock [4–6]. The intelligent perception [7–10] of the mechanical state of the surrounding rock was gradually combined with bolt support [11]. One of the key research topics is the inversion of the axial load of rock bolts.

The inversion of the axial load of a bolt can be divided into two methods: direct and indirect measurements. Among them, direct measurement of the axial load of a bolt focuses on the development of bolts with various coupled sensors [12]. Originally, the coupler load cell was arranged on the bearing plate to monitor the axial load of the bolt. Electrical-resistant strain gages have become the primary tool used by scholars to monitor the axial load of bolts. However, electricity-resistant strain gages are prone to damage during the installation and use of rock bolts, so they have been gradually replaced with additional sensors [13]. Therefore, vibrating-wire strain gages and metal-based strain gages are used instead of electricity-resistant strain gages to overcome the above shortcomings [14]. In

addition, a growing number of scholars have started to improve this work by using fiber grating sensors [15–17]. On this basis, a distributed Brillouin sensor was also proposed to monitor the axial load of rock bolts [18]. Furthermore, Vlachopoulos et al. [19] attempted to monitor the axial load of rock bolts by using distributed optical strain sensing (DOS) technology developed with a Rayleigh optical frequency domain reflectometer. Tang et al. [20] mounted a quasidistributed fiber grating sensor on a slotted anchor rod and packaged it with epoxy to hold the fiber grating sensor while monitoring the axial load. Wang et al. [21] designed a full-bar fiber grating force measurement bolt and system on the basis of the fiber grating sensing principle. However, it has always been difficult to measure the axial load of a rock bolt via a sensor to meet practical engineering requirements.

As a result, numerous methods have been developed to construct a computational model of the axial load of a rock bolt through some of the observed parameters. Cai et al. [22] used the installation time, bolt length, and deformation modulus of a rock mass as the main parameters to predict the axial load in grouted rock bolts for soft rock tunneling. Jalalifar [23] constructed an axial load prediction function based on the parameters of bolt length, interface shear stiffness, ground stress, the presence of panels, and the length of the bolt. Korzeniowski et al. [24] established a detailed dependence between the geometrical parameters of a rock bolt and the percentage of total displacement and deformation due to component deformation by removing the stress–strain feature of the bolt support. Li et al. [25] developed a different nonlinear response model that can predict both the linear elastic properties and the nonlinear response of a bolt to model the load displacement properties of the bolt. Zhang et al. [26] developed an analytical model that takes into account the varying patterns of shear stress and axial force. Zhao et al. [27] established a fully anchored bolt–surrounding rock interaction model and derived analytical expressions for the axial force and shear stress of a fully anchored bolt during normal support and critical failure. Li et al. [28] developed an analytical model to simulate the load-displacement performance of rock bolts under axial loading on the basis of the modified continuous yielding criterion. Yao et al. [29] simplified the effect of each rock bolt on the surrounding rock into two identical concentrated forces in opposite directions and provided a viscoelastic analytical solution of the axial force of the rock bolt on the basis of the complex variable method and the correspondence principle. However, the way in which the analytical model is constructed requires simplifying the actual working conditions, and the computational parameters are too few to be easily applied to practical engineering.

In contrast to the above methods, several indirect measurements have been proposed in recent years to quickly obtain the axial load of a rock bolt. In this type of approach, the bearing plate of a rock bolt, as an essential supporting element, indirectly assumes the role of the axial load of the rock bolt [30]. On the basis of these results, a series of studies with the purpose of inverting the axial load of a rock bolt and bearing plate as the subject has also been conducted. These achievements include the detection of the bearing plate [31], the processing of measurement data [32], and the inversion of loads [33].

Consequently, we propose a novel approach for the inversion of axial loads that integrates the aforementioned processes. This method is founded on the latent relationship between the axial load of the anchor bolts and the deformation of the plates, which presents a computational model for the inversion of axial load on the basis of the strain of the plates and validates the model through finite element analysis and indoor physical experiments. By integrating the computational model with the DIC method, a new inversion approach for the axial load of anchor bolts applicable to engineering practice has been proposed and tested in field experiments. The research outcomes of this paper offer new means for monitoring the mechanical state of surrounding rock in actual mining operations.

## 2. Mechanism of Axial Load Inversion Based on an Anchor Bolt Plate

This section mainly establishes an inverse mechanical theoretical model of anchor bolt loading and plate strain. By incorporating the working mechanism of the anchor bolt plate and the surrounding rock, a simplified mechanical model is constructed, and the

boundary conditions and key indicators are considered. The inversion model is established according to the basic principles of anchor bolt plate load inversion and the evolution law of surface strain.

### *2.1. The Fundamental Principle of Axial Load Inversion Based on an Anchor Bolt Plate*

Load inversion is established on the basis of the relationship between the surface strain distribution and the internal loading conditions. Through surface strain measurements, the surface strain distributions of the rock surrounding the roadway and the anchor bolt plate under different loading conditions can be acquired. The estimated values of the internal loading conditions can subsequently be obtained via the inversion algorithm.

In the roadway, the end of the anchor bolt typically withstands a considerable tensile force, which is transferred to the coal or rock mass near the anchor bolt's fixation point through the elongation of the anchor bolt. Owing to the strength constraints of the coal or rock mass, the magnitude of the tensile force of the anchor bolt generally cannot be too large; otherwise, it is prone to failure of the coal or rock mass.

To compute the relationship between the tensile force at the end of the anchor bolt and the surface strain of the bolt plate, multiple factors need to be considered, such as the elastic modulus of the anchor bolt material, the diameter of the anchor bolt, the length of the anchor bolt, the anchoring length of the anchor bolt, the friction coefficient between the anchor bolt and the rock mass, the deformation of the coal or rock mass, the stiffness of the bolt plate, etc. These factors have crucial influences on the accuracy and reliability of the model.

As shown in Figure 1, suppose that the pressure on the surface of the plate has a uniform distribution, the elastic modulus of the anchor bolt is $E$, the diameter is $d$, the length is $L$, the anchoring length is $L_0$, the friction coefficient between the rock mass and the anchor bolt is $\mu$, and the stiffness of the plate is $k$. Suppose that the tensile force exerted on the end of the anchor bolt is $F$ and that the pressure on the surface of the plate is $P$, then the following system of equations can be listed [34]:

$$F = k(\delta_{\max} - \delta_0), \tag{1}$$

$$\delta_0 = \frac{FL_0}{EA}, \tag{2}$$

$$\delta_{\max} = \frac{FL}{EA} + \frac{PL}{EA} - \frac{F\mu(L - L_0)}{A}, \tag{3}$$

where $\delta_0$ represents the strain of the anchorage portion of the anchor bolt, $\delta_{max}$ denotes the maximum displacement of the free portion of the anchor bolt, and $A$ indicates the cross-sectional area of the anchor bolt. Based on the aforementioned equation set, the relationship between $F$ and $P$ can be derived.

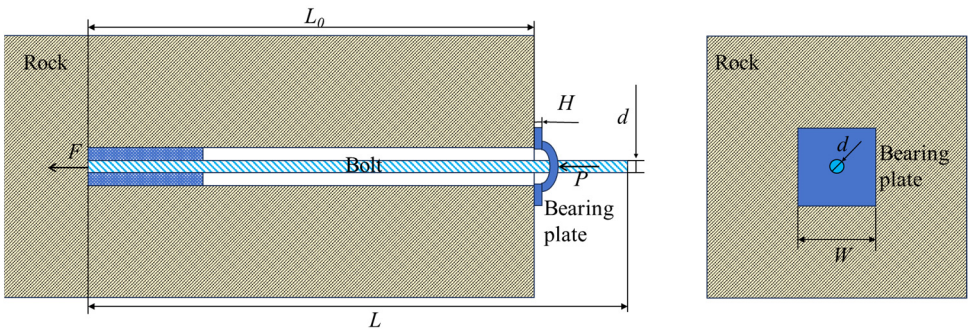



**Figure 1.** Diagram of the relation between the axial force of a rock bolt and the deformation of its bearing plate.

Supposing that the materials of both the anchor bolt and the plate are linear elastic, the relationship between strain and stress can be derived in accordance with Hooke's Law:

$$\varepsilon = \frac{\sigma}{E}, \tag{4}$$

where $\varepsilon$ denotes strain, and $\sigma$ indicates stress. The stress exerted on the anchor bolt is as follows:

$$\sigma = \frac{F}{A}, \tag{5}$$

$$\varepsilon_1 = \frac{\sigma_1 L}{Ed}, \tag{6}$$

$$\varepsilon_2 = \frac{\partial \omega}{\partial x}, \tag{7}$$

where $A$ is the contact area between the anchor bolt and the plate, $F$ is the axial load, $w$ is the deflection of the plate. The strain on the surface of the plate affected by the anchor bolt is as follows:

$$\varepsilon_3 = \frac{\varepsilon_1}{h} \cdot x, \tag{8}$$

where $h$ is the distance between the anchor bolt and the plate. $x$ denotes the horizontal distance from the anchor bolt on the plate surface. The sum of the above three strains yields the total strain on the plate surface as follows:

$$\varepsilon = \varepsilon_2 + \varepsilon_3 = \frac{\partial \omega}{\partial x} + \frac{\varepsilon_1}{h} \cdot x. \tag{9}$$

This formula delineates the relationship between the strain generated by the load on the anchor bolt and the strain on the surface of the plate and can be employed to compute the strain distribution on the plate surface. Importantly, this formula is applicable only to the simplified model; thus, adjustments and corrections need to be made in combination with the actual circumstances.

### *2.2. Axial Load Inversion Model Based on the Surface Strain Evolution Law for Anchor Bolt Plates*

By employing the finite element inversion approach, the formula of the inversion model was deduced. It is hypothesized that the anchor bolt plate is composed of uniform material, and its stress field can be assumed under the plane stress hypothesis. When subjected to a load, the anchor bolt plate will undergo elastic deformation, generating strain on its surface, thereby enabling the inversion of the load condition of the plate.

Supposing that the surface strain of the anchor bolt plate under a certain load is $\varepsilon$, the stress components in the $x$ and $y$ directions of the plate, in accordance with Hooke's Law, are as follows:

$$\sigma_x = \frac{E}{(1-\nu^2)}(\varepsilon_x - \nu\varepsilon_y), \tag{10}$$

$$\sigma_y = \frac{E}{(1-\nu^2)}(\varepsilon_y - \nu\varepsilon_x), \tag{11}$$

where $E$ is the Young's modulus of the plate, $\nu$ is the Poisson's ratio, and $\varepsilon_x$ and $\varepsilon_y$ are the strains of the plate in the $x$ and $y$ directions, respectively.

The stress components in the x and y directions act upon the two adjacent edges of the plate, so the resultant force experienced by each edge is twice the stress component. The resultant force of the plate under a certain load is as follows:

$$\begin{aligned} F &= 2(\sigma_x \cdot H \cdot L + \sigma_y \cdot H \cdot W) \\ &= 2 \cdot E \cdot H^2[\tfrac{L}{(1-\nu^2)}(\varepsilon_x - \nu\varepsilon_y) + \tfrac{W}{(1-\nu^2)}(\varepsilon_y - \nu\varepsilon_x)] \\ &= 4 \cdot E \cdot H^3[\tfrac{L}{W^3(1-\nu^2)}\varepsilon_{\max} + \sqrt{1 - (\tfrac{\varepsilon}{\varepsilon_{\max}})^2}\varepsilon] \end{aligned} \tag{12}$$

where $\varepsilon_{max}$ represents the surface strain value of the plate under the maximum load. According to the given information, when the geometric parameters of the plate are substituted into the above formula, the following equation is obtained:

$$F = \frac{4 \cdot E \cdot H^3 \cdot (1-\nu^2) \cdot \varepsilon_{\max}}{3\pi W^3} \cdot [\frac{L}{W^3} \cdot \varepsilon_{\max} + \sqrt{1-(\frac{\varepsilon}{\varepsilon_{\max}})^2}\varepsilon], \quad (13)$$

where $P$ denotes the load value derived through inversion, and the inversion model formula is obtained as follows:

$$P = \frac{4 \cdot (1-\nu^2) \cdot H^3 \cdot \varepsilon_{\max}}{3\pi W^3 \cdot (1-2\nu)} \cdot \sqrt{1-(\frac{\varepsilon}{\varepsilon_{\max}})^2}. \quad (14)$$

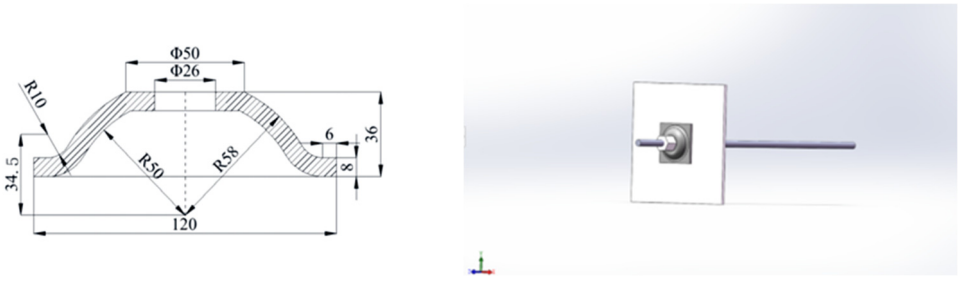
As a result, we elucidated the mechanism of axial load inversion based on anchor bolt plate.

## 3. Finite Element Analysis

In this section, ANSYS R15.0 numerical simulation software is employed to research the axial load inversion model of the rock surrounding the mining roadway.

### *3.1. Establishment of the Finite Element Model and Simulation Scheme*

The design dimensions of the spherical arched plate for the finite element analysis are 120 mm × 120 mm × 8 mm, and the specific parameters are presented in Figure 2a. The three-dimensional model of the overall experimental assembly was modeled via SolidWorks and imported into ANSYS R15.0 software. The established three-dimensional model is shown in Figure 2b.




(**a**) (**b**)

**Figure 2.** (**a**) Plate model dimensions and (**b**) simplified three-dimensional model of the anchored structure.

Subsequently, the three-dimensional model of the pallet was imported into the ANSYS numerical simulation software for intelligent meshing, with ESIZE = 0.005 m for guidance. Finally, the element type was selected. Here, SOLID186 element was chosen. SOLID186 element is a high-order three-dimensional 20-node structural solid element that permits quadratic displacement. It is mainly suitable for cases where the generated mesh model is irregular. Simultaneously, it possesses numerous practical functions such as plasticity, hyperelasticity, creep, large deformation, and large strain. The yield criterion is the von Mises criterion, namely the stress intensity invariance criterion. The plate material adopted is Q235 ordinary carbon structural steel, with a density of 7.85 × $10^3$ kg/$m^3$, Poisson's ratio υ = 0.25~0.33, elastic modulus E = 200~210 GPa, tensile strength of 370~500 MPa, and yield strength of 235 MPa. During the calculation, the elastic modulus of the plate is taken as 200 GPa, and Poisson's ratio is taken as 0.3. Since the yield strength of Q235 ordinary carbon structural steel decreases as its thickness and radius increase, the selected plates are generally no more than 16 mm. In the calculation, the yield strength of the plate should be 235 MPa.

A steel plate was employed to simulate the surrounding rock behind the bolt plate, and displacement constraints in three directions were imposed on the entire model. The loading mode of the model was time loading, with a loading step length of 10 s. Loads were applied at the ends of the anchor bolts. Finite element calculations were conducted to analyze the stress distribution and displacement deformation of the bolt plate.

### *3.2. Results of Finite Element Simulation*

The bottom surface of the bolt plate is in direct contact with the surrounding rock and is directly subjected to force to simulate the distribution of the surface load. The experimental results are shown in Figures 3 and 4. Figures 3 and 4 show that when the bolt plate is subjected to a load, the strain distribution on the surface of the bolt plate is rather complex, presenting multiple local areas of concentrated strain. The positions and magnitudes of these strain concentration areas change accordingly with the variations in the load magnitude and position, and the strain variation patterns at different positions also differ, showing distinct annular regions. The Von Mises stress nephogram coincides with the local concentrated strain areas, and within a certain range, as the load increases, the equivalent stress and strain gradually increase, and the experimental results are more evident.

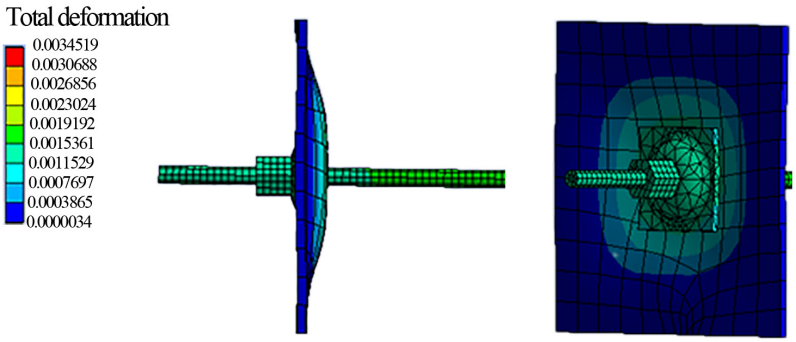



**Figure 3.** Nephogram of total deformation.

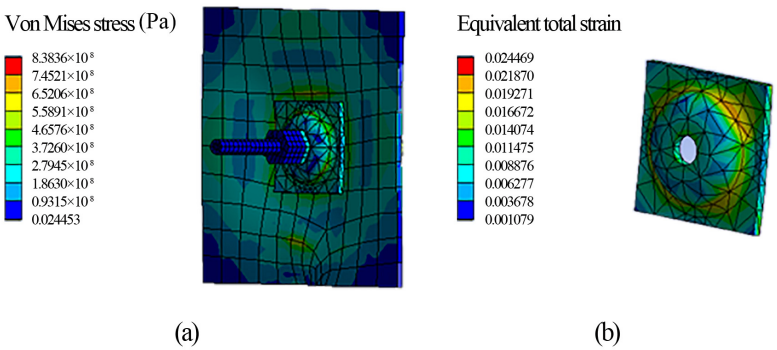



**Figure 4.** Nephograms of (**a**) Von Mises stress and (**b**) equivalent total strain.

Under different axial tensile forces of the anchor bolts, two sets of stress–strain curves, as depicted in Figure 5, are plotted, enabling the acquisition of the corresponding result analysis of plate performance. First, before a surface load of 100 kN is applied to the plate, the curves demonstrate typical linear behavior, with the yield point located at a strain of approximately 0.0005 m and the peak stress at approximately 270 MPa. The nonlinear behavior of the curves is attributed mainly to the nonlinear characteristics of the material itself. Compared with the theoretical prediction, the numerical simulation results indicate certain deviations, which might be caused by factors such as the nonuniformity of the material and the geometric shape.

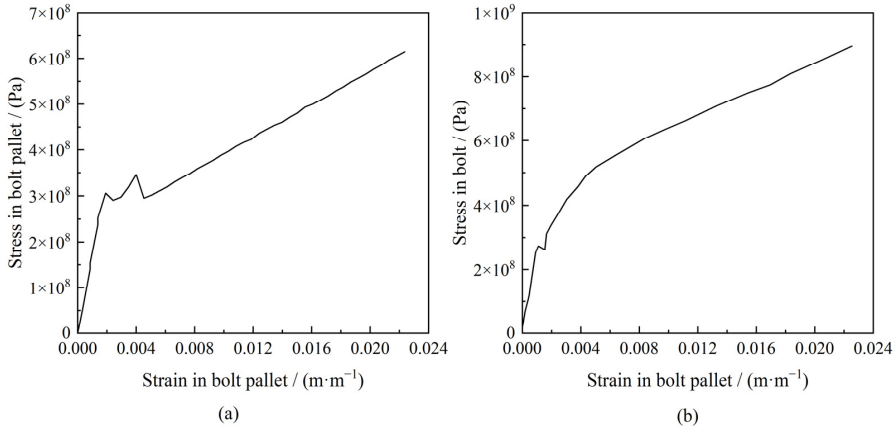



**Figure 5.** (**a**) Stress-strain curve of the plate and (**b**) stress–strain curve of the anchor bolt–plate.

It can also be observed from the curve that after the linear phase, as the load gradually increases, the slope of the graph decreases. That is, under high-intensity conditions, the degree of deformation is lower, indicating the characteristics of plastic deformation. Furthermore, when the stress and strain distributions under different loading conditions were analyzed, the stress and strain at the bottom of the plate were relatively uniform, whereas the stress and strain distributions at the end of the anchor bolt were relatively large and increased with increasing loading load. These results provide a significant reference for the design and optimization of anchor bolt–plate systems.

By comparing the stress–strain curves of the plate under the surface load distribution and the stress–strain curve of the anchor bolt–plate, it can be concluded that under the condition of ensuring the same equivalent total strain, including the elastic and plastic phases, the plate has a relatively greater relative stress when it enters the plastic phase, has a better bearing capacity, and shows a distinct oscillation trend of increasing and decreasing. The time to reach the optimal bearing performance is also later than that of the anchor bolt. The anchor bolt, as the primary force-bearing component, has a smaller corresponding yield strength and reaches the yield point earlier.

Figure 6 presents the stress–strain curves of the anchor bolt and the arch of the plate. As analyzed previously, the junction between the arch of the plate and the base plate is the strain concentration area. Research on the deformation of this area will be more effective. When the anchor bolt stress is the same, the strain of the arch of the plate has the same trend as the overall strain, and the numerical values are close. This further proves that the strain occurring in the arch of the plate plays an important role in the overall deformation of the plate.

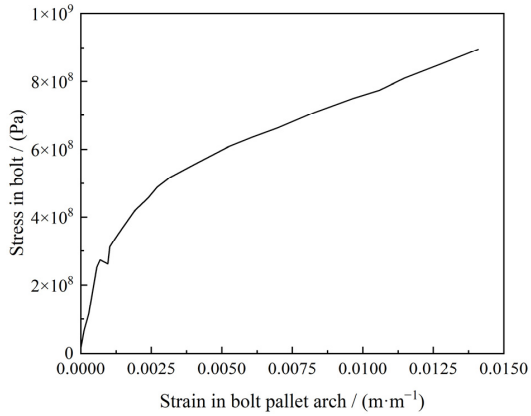



**Figure 6.** The stress–strain curve of the anchor bolt and the arch of the plate.

### *3.3. Fitting and Verification of the Load Inversion Model for Anchor Bolt Plates*

On the basis of the evolution law of surface strain, this paper presents an anchor bolt plate load inversion model based on the inversion model. The surface strain data and the stress–strain curves under different influencing factor conditions were obtained through numerical simulation, the surface strain was transformed into the load distribution of the anchor bolt plate via the inversion model, and the comparison results are shown in Figure 7.

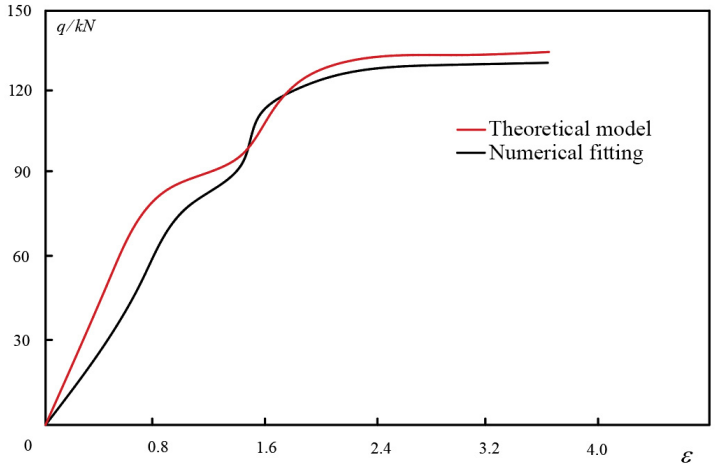



**Figure 7.** Comparison of the theoretical model and simulation experimental results for the relationship between the anchor bolt load and disc strain.

The results shown in Figure 7 are analyzed. Under the same state, the stress–strain curves of the numerical simulation are not completely consistent with the results established by the theoretical stage physical model. The strain generated in the post-peak section of the numerical simulation is earlier than that of the physical model curve, but the evolution laws of the two curves are basically the same, namely, the different periods of consolidation elasticity, plastic yield, and strengthening. Research has indicated that the anchor bolt plate load inversion method, which is based on the evolution law of surface strain, has high feasibility and practicability. However, there are still certain errors in the inversion results, and the inversion model needs to be further optimized.

## 4. Physical Experiments and Model Applications

After the rock bolt axial load inversion model was constructed on the basis of the plate strain, its validity was preliminarily verified on the basis of finite element analysis. Furthermore, this section conducts verification through indoor physical experiments and proposes a new axial load inversion method combined with the digital image correlation method while conducting tests in the engineering field.

### *4.1. Load Inversion Model Validation via Dynamic High-Speed Data Acquisition System*

On the basis of the outcomes of the finite element analysis, the reliability of the research presented in this paper can be tentatively validated. To conduct partial verification, an indoor experiment is carried out in this section. The load deformation law can be divided into stages, and characteristic observations can be conducted. In this experiment, strain gauges are affixed to the surface of the plate, and a dynamic high-speed data acquisition system (DHDAS) dynamic signal testing system is utilized for measurement during the loading process. This method aims to observe the stage characteristics and mechanical action mechanism of the load deformation law of the anchor plate. This enables verification of the load inversion method of the anchor plate and analysis of its strain evolution law.

As depicted in Figure 8, the experiment employs several anchors with a diameter of 20 mm, several Q235 common carbon structural steel plates of size 120 × 120 × 8 mm, a pull-out anchor test bench (comprising two steel plates and two steel tubes), an anchor

dynamometer, a pull-out instrument, a DHDAS dynamic signal testing and analysis system, and several strain gauges. Two approaches (quadrangle orthogonal and four-edge orthogonal, as illustrated in Figure 9) are employed to affix the strain gauges onto the plate. The plate is the object under test in the experiment, and strain measurement on it is necessary. For accurate measurement, two distinct methods for attaching strain gauges are needed.

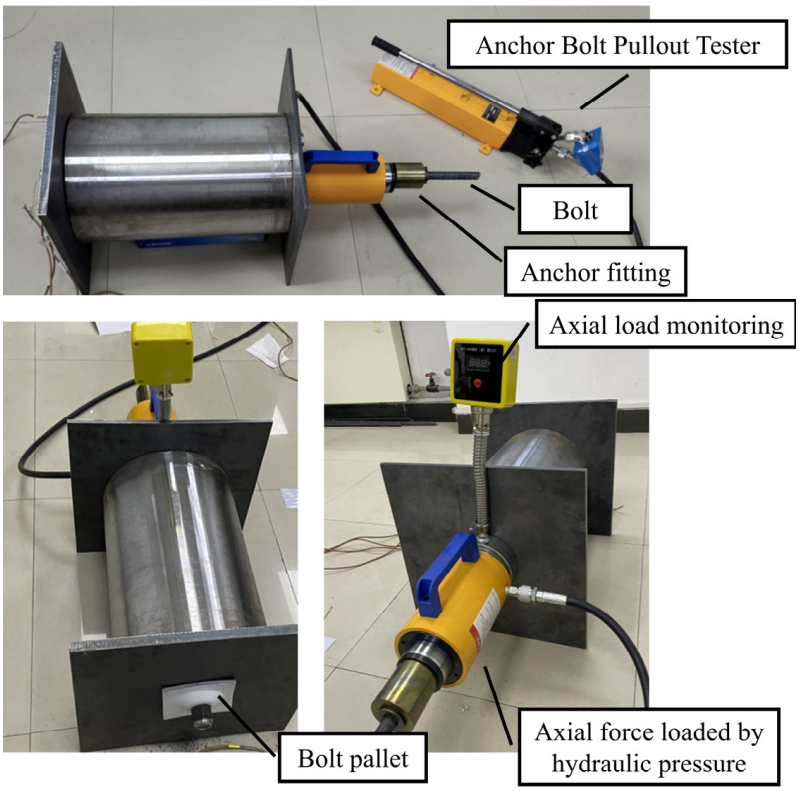



**Figure 8.** Experimental platform.

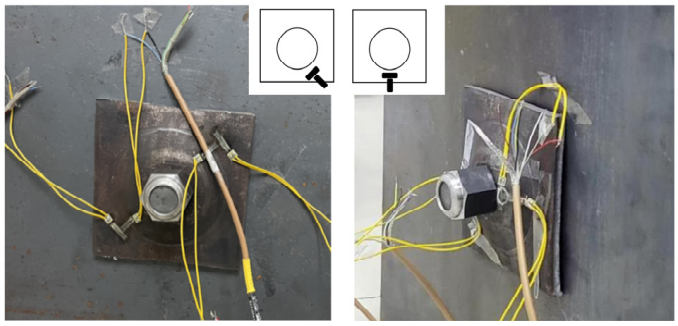



**Figure 9.** Locations of the plate and strain gauges (**a**) quadrangle orthogonal and (**b**) four-edge orthogonal are employed to affix the strain gauges onto the plate.

The data were exported through the DHDAS dynamic signal test and analysis system, and the stress–strain curves were plotted on the basis of the experimental results. As shown in Figure 10, the stress–strain curves derived from the four-sided orthogonal pasting method and the four-corner orthogonal pasting method are presented. The stress–strain curves indicate that there are numerous similarities in the deformation of the plates when the four-corner orthogonal pasting method and the four-sided orthogonal pasting method are used. Both exhibit a strain of approximately 1.6 when the stress reaches the yield point.

The dissimilarity between the two methods lies in the fact that the deformation of the arch of the plate via four-sided orthogonal pasting is more uniform. In contrast, for the plate with four-corner orthogonal pasting, the strain is greater at the same radius from the center of the hole. Since the pasting positions are located at the junction edge of the arch and the flat plate, the actual deformation displacement is larger, and the rigid displacement is smaller (mostly concentrated at the lifted corners of the flat plate). Owing to the relatively large size of the plate baseplate, when the load causes the plate to deform, it triggers a favorable yielding effect. Moreover, the significant deformation is concentrated mainly in the arch and the bottom of the arch, with less diffusion at the four sides of the baseplate. The deformation of the arch has a negligible influence on the bottom surface, and the force exerted on the arch is more uniform. To conduct further comparative observations of the plate deformation, in the experiment, the loads were applied to 80 kN, 100 kN, and 120 kN and then unloaded. The plate was removed for observation. Stages I, II, and III in Figure 10b correspond to the deformation of the plate in Figure 11. This experiment can further validate the reliability of the load inversion model and the outcomes of the finite element analysis.

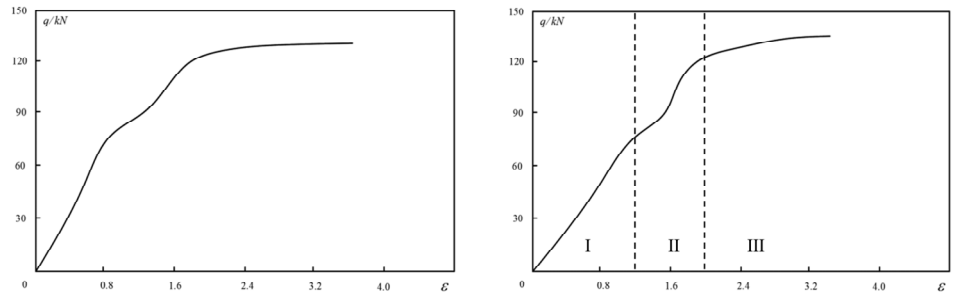



**Figure 10.** Load–strain relationship curves of the anchor bolt and plate: (**a**) four-corner orthogonal pasting method; and (**b**) four-sided orthogonal pasting method. Stages I, II, and III correspond to the deformation of the plate under 80 kN, 100 kN, and 120 kN.




**Figure 11.** Deformation states of plates under various loads.

### *4.2. A Novel Axial Load Inversion Method for Rock Bolts Based on Digital Image Correlation*

On the basis of the proposed axial load inversion model based on plate strain, a method for axial load inversion based on digital image correlation (DIC) is presented in this section. The DIC method is a strain measurement method based on optical principles that uses the deformation of speckle images to calculate surface strain. When the surface of an object is subjected to strain, the position and shape of the speckle pattern change. By analyzing the changes in the speckle image, the magnitude and distribution of surface strain can be calculated.

As depicted in Figure 12, the application mode of the DIC method in the inversion of the axial load of anchor bolts is presented. During the stereoscopic ranging process, the ranging device requires calibration. The calibration devices can be classified into two types: calibration discs of different sizes and calibration crosses. Prior to calibrating the object, calibration must be conducted on the calibration object, and the calibration results should be entered into the calibration system. In the calibration operation, the necessary geometric

parameters, such as the fixed position and orientation of each camera, can be obtained through the multiple calibration photos captured. Moreover, the imaging characteristics of each camera lens and camera chip can be determined. The measurement distance was 235 mm, and a total of twenty photos were taken. During the process, the calibration plate was rotated and tilted by 5 degrees along the horizontal and vertical axes, and ten images were captured for each. This was implemented to calibrate the cameras. Additionally, the plate needs to undergo speckle coating treatment.

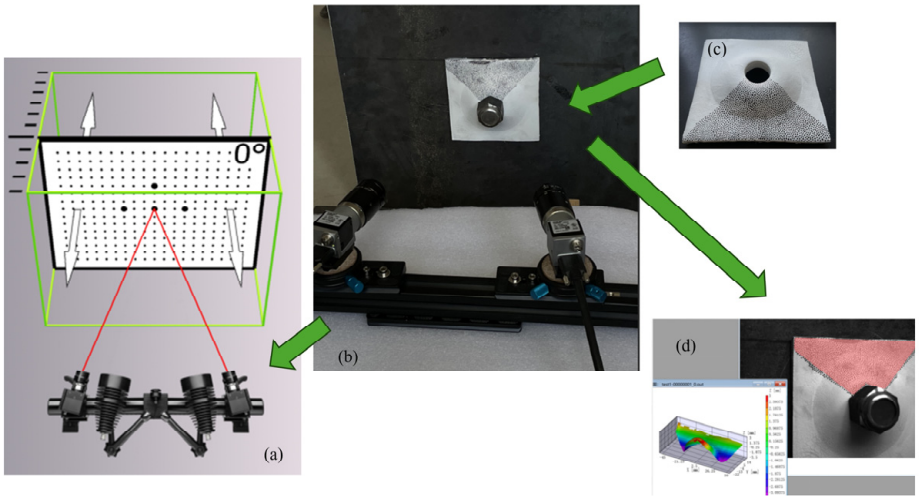



**Figure 12.** The application mode of the DIC method in the inversion of the axial load of anchor bolts: (**a**) device calibration; (**b**) data collection; (**c**) speckle coating treatment; and (**d**) data processing and analysis.

After the height adjustment, selection and debugging need to be carried out on the software. When creating the selection area, the Aoi tool of the software can select the appropriate region. When delineating the key area of interest with the lasso, it is essential to guarantee that the number of spots in the divided area grid is approximately equal and that the situation of disconnected spots should be minimized as much as possible. The preliminary debugging of the three-dimensional spatial simulation is subsequently conducted on the basis of parameters such as the step size.

As shown in Figure 13, the DIC data collected during the anchor pull-out test are presented, among which (a–d) are the strain nephograms of the plate in the U direction and (e–h) are the strain nephograms of the plate in the W direction. The spatial variation nephograms indicate that there are several obvious phenomena of sharp increases or sharp decreases in strain during the loading process of the sample, which correspond to the changes in the load at each location. Therefore, by adopting the elongation pin method for each location of the arch and the bottom surface, the typical directional strain nephograms of each location are extracted, and the global strain evolution process is analyzed.

As depicted in Figure 14, the compressive strain curves at the bottom plate of the plate adjacent to the arch and the overall compressive strain curve spanning the arch and the bottom plate are included. As represented in Figure 15, the tensile strain curve at the junction is shown. It can be concluded from the graphs that when the bottom plate and the arch of the plate are considered independently, the strains both have distinct stagewise differences of increase and decrease. However, when viewed as a whole, the overall strain trend of the plate is consistent with the results obtained from previous simulations and experiments.

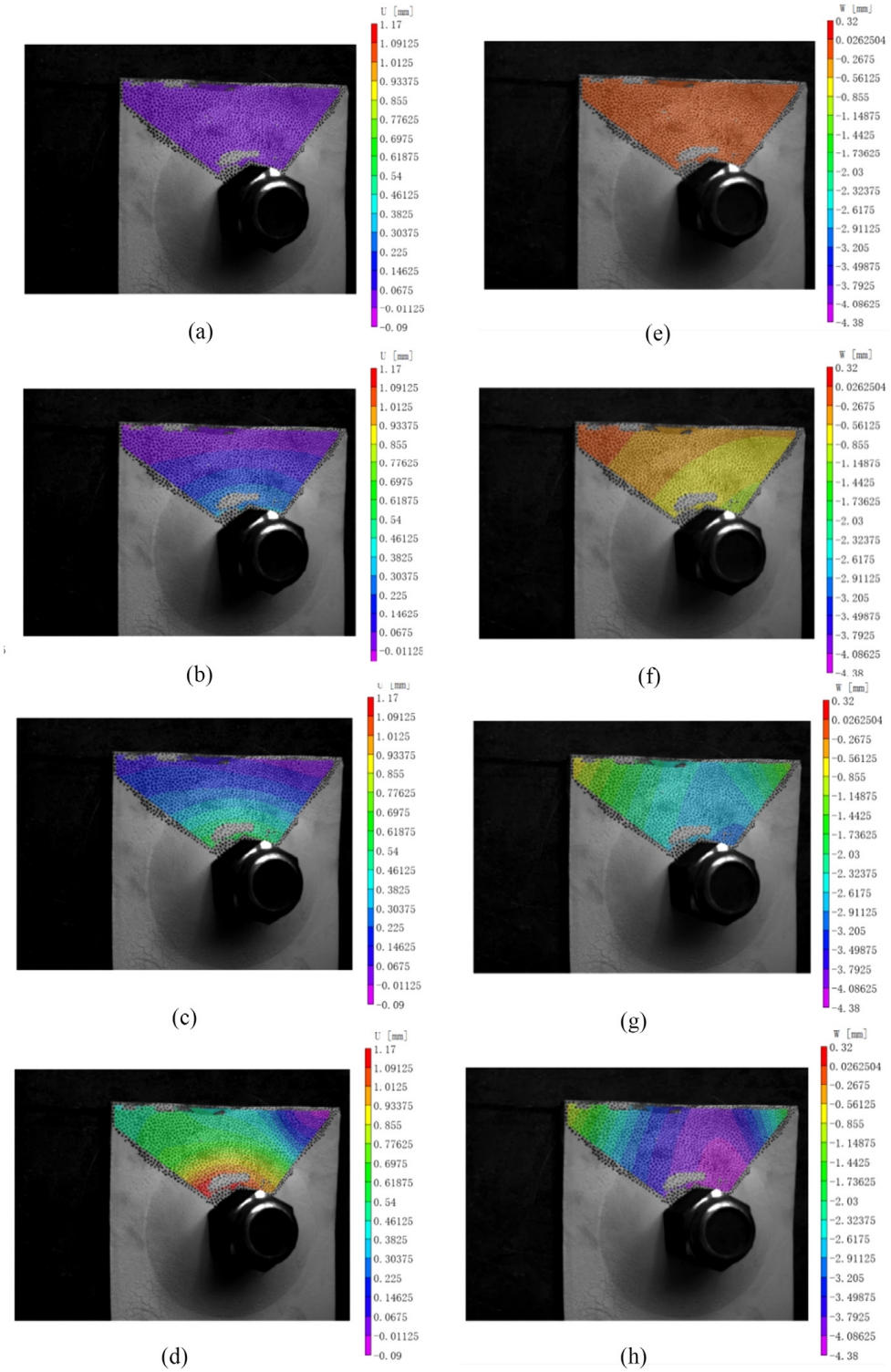



**Figure 13.** DIC data, where (**a**–**d**) are the strain nephograms of the plate in the U direction, and (**e**–**h**) are the strain nephograms of the plate in the W direction.

Prior to 40 s of data collection, the strain at the bottom plate of the sample and the junction between the arch and the bottom plate first rapidly increased. However, the overall compressive strain of the plate, represented by the green color, underwent no substantial change. The strain of the sample over a wide range remains at −0.0005. Moreover, under the initial load, there is partial eccentric compression on the W-axis.

After 40 s, as the compressive deformation of the plate becomes uniform, the eccentric compression gradually decreases.

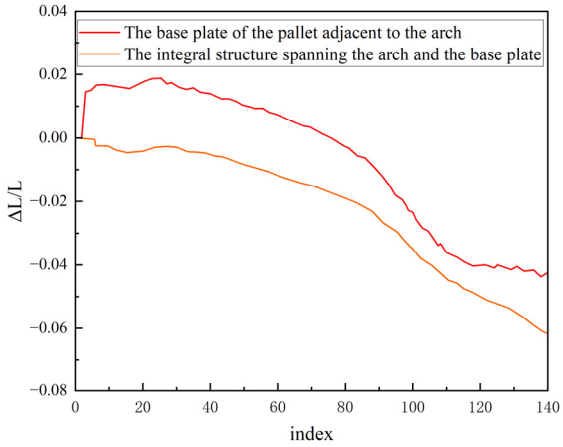



**Figure 14.** The compressive strain curves at the bottom plate of the plate adjacent to the arch and the overall compressive strain curve spanning the arch and the bottom plate are included.

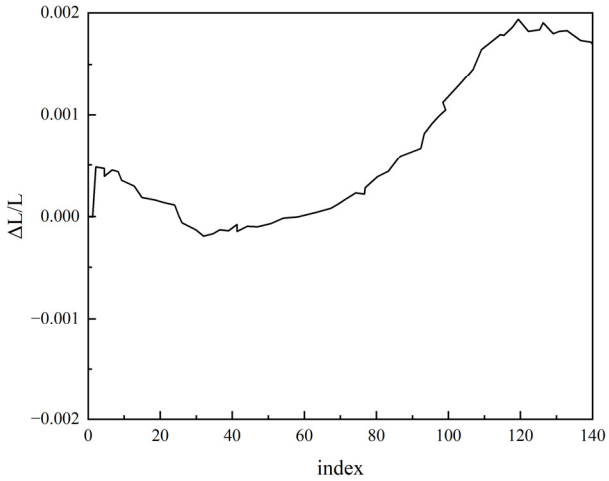



**Figure 15.** Tensile strain curve at the junction.

During the subsequent period, during the continuous loading process, the strains at the bottom plate and the junction increase continuously in positive and negative values, respectively. At the detected extension pins E0 and E1, the strain growth rates are much greater than those at the detected extension pin E2. This finding indicates that during the detection process, considerable deformation occurs near the bottom of the arch. When the 125th image was collected, the large-scale compressive strain of the plate increased to −0.005, and the local tensile strain growth reached 0.002. The maximum tensile and compressive strains were concentrated beneath the bottom of the arch. Thereafter, the descent rate of the large-scale compressive strain of the plate reached −0.006 and reached a limit. The local tensile strain at the junction of the arch bottom and the plate decreased to 0.0018, but there was still a small-scale increase. This indicates that the large-scale deformation of the plate decreased, whereas the local deformation still increased.

When the plate performs a bearing function in the bolt support, the overall deformation increases approximately uniformly over time. In terms of the subdivided stages, compression deformation is relatively rapid in Stages I and III, and plastic deformation is slower in Stage II. Nevertheless, the entire process remains in a compressive state. The plate arch and the junction between the arch and the base plate exhibit an obvious change in strain from tensile strain to compressive strain, suggesting that the bearing performance

of the plate arch is favorable and that it undertakes the main deformation of the plate. In terms of the corresponding time, the optimal point of the bearing performance of the plate is also the same as the stage determined previously. Therefore, the inversion of the axial load of the anchor bolt can be achieved via the DIC method.

### *4.3. Field Test and Engineering Application*

The excavation roadway of the outer return airway of the 122,109 fully mechanized mining face in a certain coal mine is located in the 12th panel of the 2-2 coal seam. The opening coordinates are X = 42,676,429.911 and Y = 37,403,093.400, with an azimuth of 226°30′00″. In the underground working face, the eastern part consists of four main roadways serving the entire mine. The western side is adjacent to the coal pillar at the boundary of the minefield. The southern part is the 122,111 working face (designed), and the northern part is the 122,107 working face (designed). The roadway is utilized mainly for return air and material transportation during the mining process of the 122,109 fully mechanized mining face in the 12th panel.

During the production process, the roof is jointly supported by a 6000 × 1100 mm reinforcing mesh, Φ20 × 2000 mm threaded steel bolts, and Φ17.8 × 6500 mm anchor cables. The spacing between the top bolts × row spacing = 1000 × 1000 mm, and 6 bolts are used for each row of support. The spacing between the anchor cables × row spacing = 2000 × 3000 mm. The spacing between the side bolts × row spacing = 1000 × 1000 mm. On the coal pillar side of the roadway, a combined support of Φ20 × 2000 mm threaded steel bolts and plastic nets is adopted, whereas, on the noncoal pillar side of the roadway, Φ20 × 2000 mm fiberglass bolts are used for support. The actual construction situation of the support engineering is depicted in Figure 16.



(a) (b)

**Figure 16.** The supporting conditions at the engineering site. (**a**) Installation of rock bolts, (**b**) Rock anchor after receiving load.

The loads collected through real-time DIC observations were compared and analyzed with the measurements of the onsite anchor bolts (as shown in Figure 17). During the plastic stage, errors may arise due to large deformations. The influencing factors observed have certain time effects and influence rigid body rotation. By eliminating rigid displacements, precise and real-time recording of deformations can be achieved through photography, thus attaining a favorable engineering support effect.

The results are listed in Table 1. The pretensioning forces of both the roof-threaded steel anchor bolts and the threaded steel anchor bolts at the coal pillar side fulfilled the design requirements; that is, no anchor bolts were pulled off or broken. The measured load values of the roof anchor bolts have relatively small differences from the values measured by digital speckle in the field, both of which are approximately 100 kN. Nevertheless, considering the adjustment of the alignment between the anchor bolts and the plates after

the pretensioning force is applied, the pretensioning force of the anchor bolts slightly decreases. Hence, the mining party should appropriately increase the application standard of the pretensioning force during the construction of the roof anchor cables to ensure that the subsequent pretensioning force meets the design requirements. By observing the load indications of the anchor bolts on both the left and right sides, the anchoring forces at the sidewalls also met the design requirements, and no anchor cables were pulled off or broken. The above results can be analyzed intuitively to conclude that the relevant methods of digital speckle combined with the inversion model from theoretical research can accurately record deformations in real time and infer and evaluate the working status and support effect in mine support, which holds certain practical significance.



**Figure 17.** Measuring the actual axial load of the anchor bolts.

**Table 1.** Comparison between the measured load and actual load.

| **Location and numbering of anchor bolts** | Left Side 1 | Left Side 2 | Left Side 3 | Top Anchor 1 | Top Anchor 2 | Top Anchor 3 | Top Anchor 4 | Top Anchor 5 | Right Side 1 | Right Side 2 | Right Side 3 |
|---|---|---|---|---|---|---|---|---|---|---|---|
| **Measured load (kN)** | 37 | 43 | 41 | 92 | 83 | 103 | 105 | 96 | 38 | 42 | 43 |
| **Actual load (kN)** | 35 | 45 | 49 | 96 | 87 | 100 | 102 | 98 | 40 | 47 | 33.5 |

## 5. Discussion

The load inversion of rock anchor bolts is an important means for evaluating the quality of coal mine support engineering and perceiving the mechanical state of the surrounding rock. The anchor bolt plate load inversion method based on the evolution law of surface strain proposed in this paper can provide powerful support for the design, construction and monitoring of anchor bolt plate structures and has extensive prospects for promotion and application. During the design and construction of anchor bolt plate structures, the inversion method proposed in this research can be employed to conduct real-time monitoring and assessment of the stress state of anchor bolt plates, promptly identify potential issues and make adjustments to enhance engineering quality and safety. The inversion method proposed in this paper can be combined with other monitoring methods (such as strain gauges, displacement meters, and acoustic wave detection) to further improve the monitoring accuracy and reliability of anchor bolt plate structures. Moreover, the inversion model and method presented in this paper have certain universality and scalability and can be flexibly adjusted and applied on the basis of the specific characteristics of engineering structures and actual circumstances. In the future, further inversion studies targeting different engineering structures and load types can be carried out to expand the application scope and accuracy of the inversion model and method and enhance its reliability and accuracy in practical engineering applications.

Moreover, the methodology of this research can also be applied to other domains, such as structural health monitoring in bridges and large-scale machinery. Through monitoring and inverting the strain distribution of structures, real-time monitoring and early warning

of the structural health status can be realized, guaranteeing the safe operation of the structures. This study has delved deeply into the load inversion of anchor plates; however, in practical applications, there are still some issues that require further resolution. For example, in complex geological conditions, there might be certain errors in the load inversion of anchor plates, which need to be addressed through further research and experiments. Additionally, in future studies, the inversion model and algorithm of this research can be further refined to improve the inversion precision and accuracy. Furthermore, a more detailed exploration is needed regarding the influence of the relevant parameters of the anchoring structure on the results, such as the length of the rock bolt [35]. Concurrently, the method of this research can be applied to a broader range of fields, providing more effective means and tools for safe operation and structural health monitoring of engineering.

## 6. Conclusions

Anchor rock bolts are among the inevitable support components employed in coal mine support engineering. Measuring the axial load of the supporting anchor bolts constitutes an important foundation for evaluating the support effect and the mechanical state of the surrounding rock. The existing methods for measuring the axial load of rock bolts have difficulty meeting the actual demands in terms of accuracy and means. Combining the working mechanism of anchor bolt plates and the surrounding rock, a simplified mechanical model of the plate was constructed by formulating a bending differential equation in accordance with the boundary conditions. On the basis of the basic principles of anchor bolt plate load inversion and the evolution law of surface strain, an inversion model was established to conduct stress–strain analysis in the elastic–plastic stage of the arched plate under force. Moreover, the inversion model was preliminarily verified and corrected on the basis of finite element analysis and indoor experiments. Furthermore, a novel application method that combines the load inversion model with the DIC method was proposed, the applied technology of this theory was presented, and the method was tested in a mine.

Through finite element analysis, it was discovered that the inversion model proposed in this paper is largely consistent with the results of its stress–strain curve. Furthermore, the results of the indoor experiment carried out via the dynamic high-speed data acquisition system are consistent with the previous results, indicating the theoretical reliability of the method proposed in this paper. The inversion model was combined with the DIC method and applied onsite. By comparing the measured load with the actual load, the average error of load inversion under different anchoring environments (left side, top anchor, and right side) was controlled within 4 kN, 3.2 kN, and 5.5 kN, respectively. The proportions of the average error to the entire load are 8.8%, 3.6%, and 14.7%, respectively. This approach is robust in actual production. Therefore, the new method for axial load inversion of rock bolts proposed in this paper provides a reliable means for evaluating the quality of mine support engineering and perceiving the mechanical state of the surrounding rock.

**Author Contributions:** Conceptualization, Y.L. and X.X.; Funding acquisition, X.X.; Methodology, Y.L. and X.X.; Project administration, X.X.; Supervision, X.X.; Validation, S.T. and H.S.; Visualization, S.T. and H.S.; Writing—original draft, Y.L. and X.X.; Writing—review & editing, S.T. and X.X. All authors have read and agreed to the published version of the manuscript.

**Funding:** This research was funded by the National Natural Science Foundation of China (Grant No. 51864044) and the Independent Research Project of State Key Laboratory of Coal Resources and Safe Mining, CUMT (Grant No. SKLCRSM21X003).

**Data Availability Statement:** The original contributions presented in the study are included in the article material, further inquiries can be directed to the corresponding author.

**Acknowledgments:** The authors would like to thank the editor, assistant editor, and anonymous reviewers for their careful reviews and insightful remarks.

**Conflicts of Interest:** Yongchao Lei was employed by the Henan Energy Group Co., Ltd. The remaining authors declare that the research was conducted in the absence of any commercial or financial relationships that could be construed as a potential conflict of interest.

## References


1. Staniek, A. Technical Problems and Non Destructive Testing of Rock Bolt Support Systems in Mines. *Int. J. Coal Sci. Technol.* **2023**, *10*, 6. [CrossRef]
2. Li, D.; Ma, S.; Lane, M.; Chang, P.; Crompton, B.; Hagen, S.A. Laboratory Investigations into the Failure Mechanisms of New Yielding and Inflatable Rockbolts Under Axial and Shearing Loading Conditions. *Rock Mech. Rock Eng.* **2023**, *56*, 565–587. [CrossRef]
3. Xue, Y.; Wang, J.; Xiao, J. Bibliometric Analysis and Review of Mine Ventilation Literature Published between 2010 and 2023. *Heliyon* **2024**, *10*, e26133. [CrossRef] [PubMed]
4. Singh, P.; Spearing, A.J.S.; Jessu, K.V.; Caroline Pinazzi da Silva Ribeiro, P. Establishing the Need to Model the Actual State of Stress Along Rock Bolts. *Int. J. Min. Sci. Technol.* **2020**, *30*, 279–286. [CrossRef]
5. Dai, L.; Xiao, Y.; Pan, Y.; Wang, A.; Fan, C.; Guo, J. Mechanical Behavior and Factors Influencing Axial Splitting Energy Absorbers and Optimized Application for Rock Bolts. *Tunn. Undergr. Space Technol.* **2020**, *102*, 103427. [CrossRef]
6. He, Z.; Xu, X.; Rao, D.; Peng, P.; Wang, J.; Tian, S. PSSegNet: Segmenting the P- and S-Phases in Microseismic Signals through Deep Learning. *Mathematics* **2023**, *12*, 130. [CrossRef]
7. Wang, J.; Xue, Y.; Xiao, J.; Shi, D. Diffusion Characteristics of Airflow and CO in the Dead-End Tunnel with Different Ventilation Parameters after Tunneling Blasting. *ACS Omega* **2023**, *8*, 36269–36283. [CrossRef]
8. Wang, J.; Xiao, J.; Xue, Y.; Wen, L.; Shi, D. Optimization of Airflow Distribution in Mine Ventilation Networks Using the Modified Sooty Tern Optimization Algorithm. *Min. Metall. Explor.* **2024**, *41*, 239–257. [CrossRef]
9. He, Z.; Jia, M.; Wang, L. UACNet: A Universal Automatic Classification Network for Microseismic Signals Regardless of Waveform Size and Sampling Rate. *Eng. Appl. Artif. Intell.* **2023**, *126*, 107088. [CrossRef]
10. He, Z.; Ma, S.; Wang, L.; Peng, P. A Novel Wavelet Selection Method for Seismic Signal Intelligent Processing. *Appl. Sci.* **2022**, *12*, 6470. [CrossRef]
11. Pinazzi, P.C.; Spearing, A.J.S.; Jessu, K.V.; Singh, P.; Hawker, R. Mechanical Performance of Rock Bolts under Combined Load Conditions. *Int. J. Min. Sci. Technol.* **2020**, *30*, 167–177. [CrossRef]
12. Song, G.; Li, W.; Wang, B.; Ho, S.C.M. A Review of Rock Bolt Monitoring Using Smart Sensors. *Sensors* **2017**, *17*, 776. [CrossRef] [PubMed]
13. Spearing, A.J.S.; Hyett, A.J.; Kostecki, T.; Gadde, M. New Technology for Measuring the in Situ Performance of Rock Bolts. *Int. J. Rock Mech. Min. Sci.* **2013**, *57*, 153–166. [CrossRef]
14. Mitri, H. Evaluation of Rock Support Performance Through Instrumentation and Monitoring of Bolt Axial Load. In Proceedings of the 11th Underground Coal Operators' Conference, Wollongong, Australia, 21 March 2011; pp. 136–140.
15. Moerman, W.; Taerwe, L.; De Waele, W.; Degrieck, J.; Himpe, J. Measuring Ground Anchor Forces of a Quay Wall with Bragg Sensors. *J. Struct. Eng.* **2005**, *131*, 322–328. [CrossRef]
16. Ho, S.C.M.; Li, W.; Wang, B.; Song, G. A Load Measuring Anchor Plate for Rock Bolt Using Fiber Optic Sensor. *Smart Mater. Struct.* **2017**, *26*, 057003. [CrossRef]
17. Weng, X.; Ma, H.; Wang, J. Stress Monitoring for Anchor Rods System in Subway Tunnel Using FBG Technology. *Adv. Mater. Sci. Eng.* **2015**, *2015*, 480184. [CrossRef]
18. Moffat, R.A.; Beltran, J.F.; Herrera, R. Applications of BOTDR Fiber Optics to the Monitoring of Underground Structures. *Geomech. Eng.* **2015**, *9*, 397–414. [CrossRef]
19. Vlachopoulos, N.; Cruz, D.; Forbes, B. Utilizing a Novel Fiber Optic Technology to Capture the Axial Responses of Fully Grouted Rock Bolts. *J. Rock Mech. Geotech. Eng.* **2018**, *10*, 222–235. [CrossRef]
20. Tang, B.; Cheng, H.; Tang, Y.; Yao, Z.; Rong, C.; Xue, W.; Lin, J. Application of a FBG-Based Instrumented Rock Bolt in a TBM-Excavated Coal Mine Roadway. *J. Sens.* **2018**, *2018*, e8191837. [CrossRef]
21. Wang, P.; Zhang, N.; Kan, J.; Xie, Z.; Wei, Q.; Yao, W. Fiber Bragg Grating Monitoring of Full-Bolt Axial Force of the Bolt in the Deep Strong Mining Roadway. *Sensors* **2020**, *20*, 4242. [CrossRef]
22. Cai, Y.; Esaki, T.; Jiang, Y. An Analytical Model to Predict Axial Load in Grouted Rock Bolt for Soft Rock Tunnelling. *Tunn. Undergr. Space Technol.* **2004**, *19*, 607–618. [CrossRef]
23. Jalalifar, H. An Analytical Solution to Predict Axial Load along Fully Grouted Bolts in an Elasto-Plastic Rock Mass. *J. South. Afr. Inst. Min. Metall.* **2011**, *111*, 809–814.
24. Korzeniowski, W.; Skrzypkowski, K.; Herezy, Ł. Laboratory Method for Evaluating the Characteristics of Expansion Rock Bolts Subjected to Axial Tension. *Arch. Min. Sci.* **2015**, *60*, 209–224. [CrossRef]
25. Li, D.; Masoumi, H.; Hagan, P.C.; Saydam, S. Experimental and Analytical Study on the Mechanical Behaviour of Cable Bolts Subjected to Axial Loading and Constant Normal Stiffness. *Int. J. Rock Mech. Min. Sci.* **2019**, *113*, 83–91. [CrossRef]
26. Zhang, W.; Huang, L.; Juang, C.H. An Analytical Model for Estimating the Force and Displacement of Fully Grouted Rock Bolts. *Comput. Geotech.* **2020**, *117*, 103222. [CrossRef]

27. Zhao, C.; Li, Y.; Liu, G.; Chen, D.; Meng, X. Research on the Stress Distribution Law of Fully Anchored Bolt and Analysis of Influencing Factors under the Condition of Surrounding Rock Deformation. *Adv. Civ. Eng.* **2020**, *2020*, e8818375. [CrossRef]
28. Li, D.; Li, Y.; Chen, J.; Masoumi, H. An Analytical Model for Axial Performance of Rock Bolts under Constant Confining Pressure Based on Continuously Yielding Criterion. *Tunn. Undergr. Space Technol.* **2021**, *113*, 103955. [CrossRef]
29. Yao, S.; Cai, H.; Lu, A. Viscoelastic Solution for Axial Forces of Point-Anchored Rock Bolts in a Circular Tunnel. *Int. J. Appl. Mech.* **2023**, *15*, 2350011. [CrossRef]
30. Wang, B.; Yu, W.; Chen, Z. Effect of Anchor Plate on the Mechanical Behavior of Prestressed Rock Bolt Used in Squeezing Large Deformation Tunnel. *Acta Geotech.* **2022**, *17*, 3591–3611. [CrossRef]
31. Gallwey, J.; Eyre, M.; Coggan, J. A Machine Learning Approach for the Detection of Supporting Rock Bolts from Laser Scan Data in an Underground Mine. *Tunn. Undergr. Space Technol.* **2021**, *107*, 103656. [CrossRef]
32. Li, C.; Xia, X.; Feng, R.; Gao, X.; Chen, X.; Lei, G.; Bai, J.; Nie, B.; Zhang, Z.; Zhang, B. Experimental Study of the Effect of Axial Load on Stress Wave Characteristics of Rock Bolts Using a Non-Destructive Testing Method. *Sustainability* **2022**, *14*, 9773. [CrossRef]
33. Liu, W.; Gao, F.; Dong, S.; Yuan, G. A Novel Method for Estimating Axial Force of Rock Bolt Through 3D Laser Scanning and Deep Learning. *Rock Mech. Rock Eng.* **2024**, *57*, 1437–1450. [CrossRef]
34. Wang, M.; Shang, L.; Zhang, B.; Li, Y.; Su, J.; Wang, S. Study on Reasonable Anchorage Length Based on Failure Mechanism of the Bolt Anchorage System. *Sci. Rep.* **2023**, *13*, 22915. [CrossRef] [PubMed]
35. Hasanzadehshooiili, H.; Lakirouhani, A.; Medzvieckas, J. Superiority of Artificial Neural Networks over Statistical Methods in Prediction of the Optimal Length of Rock Bolts. *J. Civ. Eng. Manag.* **2012**, *18*, 655–661. [CrossRef]


**Disclaimer/Publisher's Note:** The statements, opinions and data contained in all publications are solely those of the individual author(s) and contributor(s) and not of MDPI and/or the editor(s). MDPI and/or the editor(s) disclaim responsibility for any injury to people or property resulting from any ideas, methods, instructions or products referred to in the content.